Role of Renner Teller and Spin−Orbit Interaction in the Reactive Scattering of O(^{3}P) Atoms with CF$_3$I Molecules

D. D. Wells, S. Mohr, K. M. Goonan, M. Hammer, and R. Grice*

Chemistry Department, University of Manchester, Manchester, M13 9PL, U.K.

Received: March 10, 1997; In Final Form: April 30, 1997⊗

Reactive scattering of O(^{3}P) atoms with CF$_3$I molecules has been studied at initial translational energies $E \sim$ 108 and 42 kJ mol^{-1} using supersonic beams of O atoms seeded in He buffer gas generated from rf and microwave discharge sources. At the higher initial translational energy, the IO scattering shows a broad peak in the forward hemisphere with respect to the initial O atom direction with a product translational energy distribution shifted to higher energy than the prediction of phase space theory. At the lower initial translational energy, the IO scattering shows a sideways peaked component with a fraction $f' \sim 0.4$ of the total available energy being disposed into translation and a forward and backward peaked component with a product translational energy distribution in accord with the predictions of phase space theory. The sideways scattering is attributed to direct reaction over the triplet $^3A''$ potential energy surface, while the forward and backward peaked scattering is attributed to dissociation of a persistent singlet OICF$_3$ complex formed by intersystem crossing to the underlying $^1A'$ potential energy surface. The direct scattering over the triplet $^3A''$ potential energy surface contributes a fraction, ~0.5, to the total reaction cross section at the lower initial translational energy, while the forward scattering at the higher initial translational energy is dominated by direct reaction over the triplet $^3A''$ potential energy surface. This dynamical behavior is correlated with the effect of charge transfer interaction of the form OI$^+$R$^-$ on Renner Teller splitting of the triplet potential energy surface.

Introduction

Recent measurements[1,2] of the reactive scattering of O(^{3}P) atoms with alkyl iodide molecules have demonstrated the role of intersystem crossing from the initial triplet potential energy surface to the underlying singlet potential energy surface which supports a stable OIR intermediate. This yields a long-lived collision complex which dissociates either by C−I bond fission to form IO product or via a five-membered ring transition state to form HOI product.[3] Direct reaction over the triplet potential energy surface leading to IO scattering in the backward direction is observed at higher initial translational energy. Addision *et al.*[4] first suggested that the reaction of O(^{3}P) atoms with CF$_3$I molecules might involve intersystem crossing on the basis of the low rate constant measured for a reaction with a negligible activation energy in a flash photolysis experiment. Early crossed beam reactive scattering experiments[5,6] suggested that reaction proceeds via a persistent collision complex at low initial translational energy, which was attributed to reaction over the triplet potential energy surface. However, this situation was clouded by apparent discrepancies between the experimental data obtained by Gorry *et al.*[5] and that of Buss *et al.*[6] and differences in the details of their interpretation. Subsequently, matrix isolation experiments[7] have provided evidence for a stable OICF$_3$ intermediate which is analogous to the OIR intermediate[8,9] observed in the akyl iodide reactions. In order to resolve the mechanism of the reaction

$$O(^3P) + CF_3I \rightarrow IO(^2\Pi_{3/2}) + CF_3 \qquad (1a)$$

$$\rightarrow IO(^2\Pi_{1/2}) + CF_3 \qquad (1b)$$

the reactive scattering experiments have been extended up to an initial translational energy $E \sim 108$ kJ mol^{-1}, with improved velocity resolution of the IO product scattering.

TABLE 1: Beam Velocity Distributions, Peak Velocity v_{pk}, Full Width at Half-Maximum Intensity v_{wd}, and Mach Number M

beam	v_{pk}/m s^{-1}	v_{wd}/m s^{-1}	M
O(He)	3800	1200	6
O(He)	2350	890	4
CF$_3$I	370	150	5

Experimental Section

The apparatus was the same as that previously employed in the study[10] of the O + ICl reaction. A high temperature radio frequency discharge source[11] was used to produce a supersonic beam of O(^{3}P) atoms seeded in He buffer gas with peak velocity ~ 3800 m s^{-1}, while a high pressure microwave discharge source[12] was used to give a peak velocity ~ 2350 m s^{-1} for O atoms seeded in He buffer gas. The O atom beam velocity distributions were measured by using a beam monitor quadrupole mass spectrometer, yielding the parameters quoted in Table 1. The CF$_3$I beam issued from a stainless steel nozzle source of diameter ~ 0.1 mm using a stagnation pressure ~ 300 mbar. The velocity distribution of the CF$_3$I beam was measured with the rotatable mass spectrometer detector by using pseudorandom cross-correlation time-of-flight analysis[13] integrated in phase with modulation of the beam by a tuning fork chopper to gain the parameters listed in Table 1. Time-of-flight analysis of the IO reactive scattering and CF$_3$I beam velocity distribution employs channel widths ~ 10 μs, an improvement of a factor of 2 in resolution over previous measurements.[5] The absence of electronically excited O(^{1}D) atoms from the O(^{3}P) beam was checked by use of an HCl cross beam in place of the CF$_3$I beam. No ClO product scattering was observed from the reaction[14]

$$O(^1D) + HCl \rightarrow ClO + H \qquad (2)$$

Results

Angular distribution measurements of IO reactive scattering yield ~ 30 and ~ 80 counts s^{-1} against backgrounds ~ 30 and

---

⊗ Abstract published in *Advance ACS Abstracts,* September 15, 1997.

S1089-5639(97)00880-3 CCC: $14.00

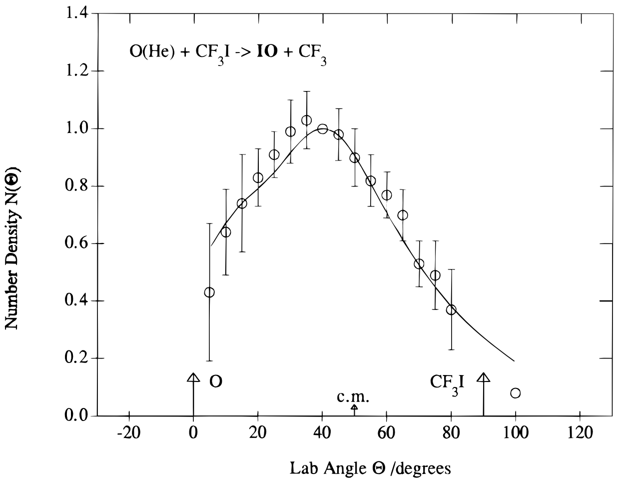

Figure 1. Laboratory angular distribution (number density) of IO reactive scattering from O + CF$_3$I at initial translational energy $E \sim 108$ kJ mol^{-1}. The solid line shows the fit of the kinematic analysis. The laboratory centroid is located at $\Theta = 50°$.

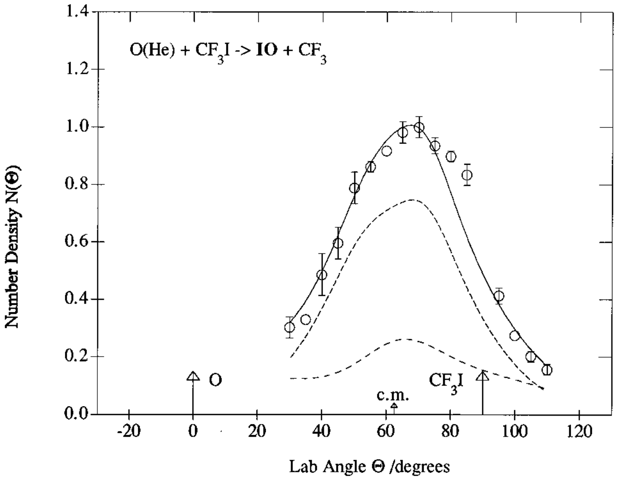

Figure 2. Laboratory angular distributions (number density) of IO reactive scattering from O + CF$_3$I at an initial translational energy $E \sim 42$ kJ mol^{-1}. The laboratory centroid is located at $\Theta = 63°$.

15 counts s^{-1} for initial translational energies $E \sim 108$ and 42 kJ mol^{-1}. The laboratory angular distributions of IO scattering in Figures 1 and 2 peak close to the centroid vector, being perceptibly shifted to wider angles at lower initial translational energy and smaller angles at higher initial translational energy. In the case of experiments with the RF discharge source, the IO signal was measured selectively in early time channels corresponding to high laboratory velocities in order to minimize interference from ambient background molecules with low laboratory velocities. The laboratory velocity distributions of IO scattering were measured by using integration times ~ 10 000 s to gain signal to noise ratios ~ 10 in Figure 3 and ~ 15 in Figure 4 at the peaks of the distributions. Kinematic analysis of these data was undertaken by using the forward convolution method[15] with the differential cross section expressed as a product of an angular function $T(\theta)$ and a velocity function $U(u)$

$$I_{\mathrm{cm}}(\theta,u) = T(\theta)U(u) \qquad (3)$$

At the higher initial translational energy $E \sim 108$ kJ mol^{-1}, the IO product scatters preferentially in the forward hemisphere in Figure 5 but at the lower energy $E \sim 42$ kJ mol^{-1} sideways peaked scattering with higher product translational energy can be distinguished from the forward and backward peaked scattering with lower product translational energy, which favors the backward direction in Figure 6. Hence the IO scattering in Figure 2 arises from a weighted sum of the two differential cross sections in Figure 6, each expressed according to eq 3. The quality of fit to the velocity distributions in Figure 3 is poorer at $\Theta = 20°$ close to the O atom beam and in Figure 4 at $\Theta = 80°$ close to the CF$_3$I beam. In each case this represents the scattering angle where the laboratory data are most subject to background noise from the adjacent beam. The peak E'_{pk} and average E'_{av} product translational energies are listed in Table 2, together with the initial translational energies E and the reaction exoergicity ΔD_0 calculated from the bond energies of IO from Radlein *et al.*[16] and Buss *et al.*[6] and CF$_3$I of Okafo and Whittle.[17]

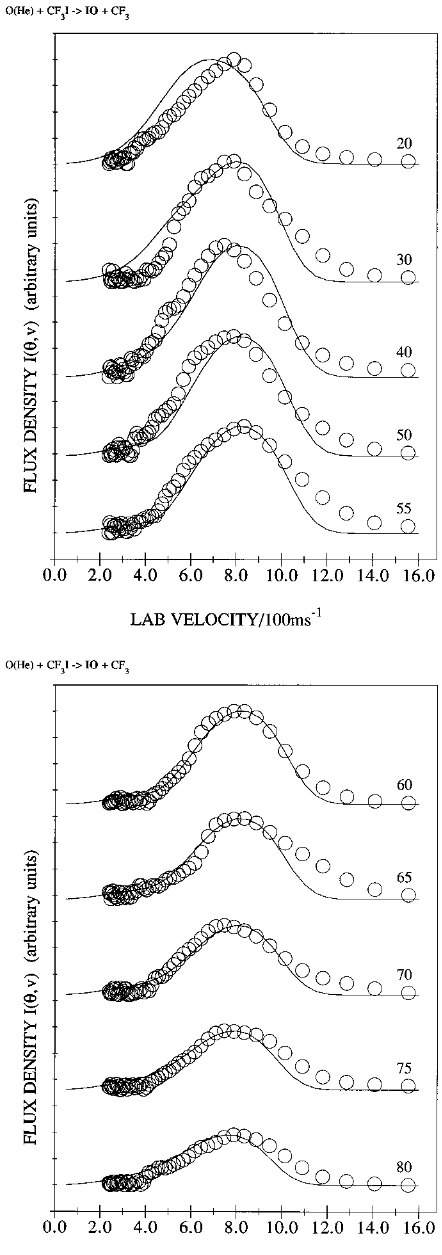

Figure 3. Laboratory velocity distributions (flux density) of reactively scattered IO from O + CF$_3$I at an initial translational energy $E \sim 108$ kJ mol^{-1}. Solid line shows the fit of the kinematic analysis and numbers denote the laboratory scattering angles. Relative errors are ~0.1 at the peaks of the distributions, increasing to ~1 at the highest and lowest velocities.

The ratio of the contributions of the two components to the total reaction cross section for IO scattering may be estimated

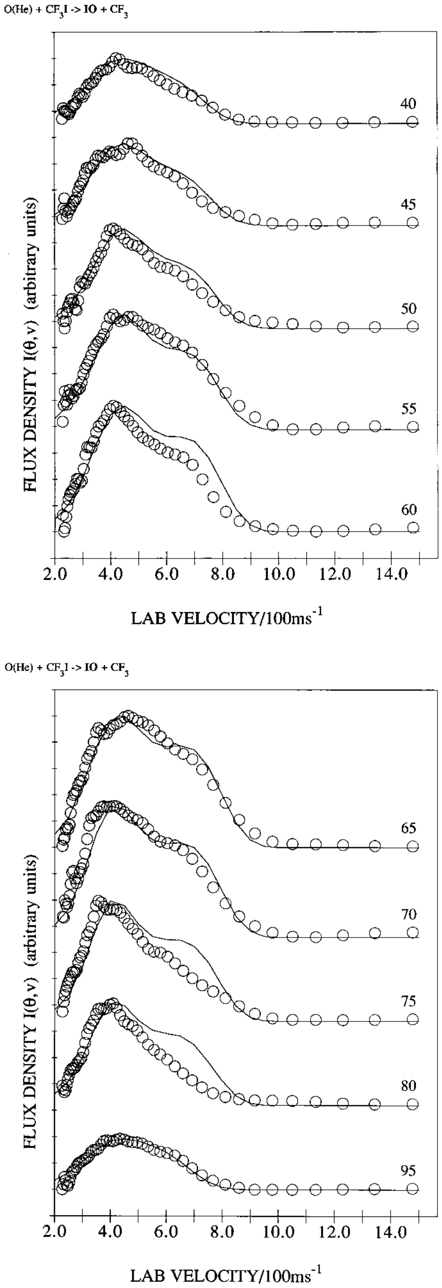

Figure 4. Laboratory velocity distributions (flux density) of reactively scattered IO from O + CF$_3$I at an initial translational energy $E \sim 42$ kJ mol^{-1}.

by integration over the differential cross sections in Figure 6

$$Q = 2\pi \int_0^{u_{\max}} \int_0^{\pi} I_{\mathrm{cm}}(\theta,u) \sin\theta \, \mathrm{d}\theta \, \mathrm{d}u \qquad (4)$$

This yields a ratio Q(fast)/Q(slow) $\sim 1.1 \pm 0.3$ for the sideways compared with the forward and backward scattered component, where the uncertainty is estimated from the leeway in the kinematic analysis of the experimental data in Figures 2 and 4.

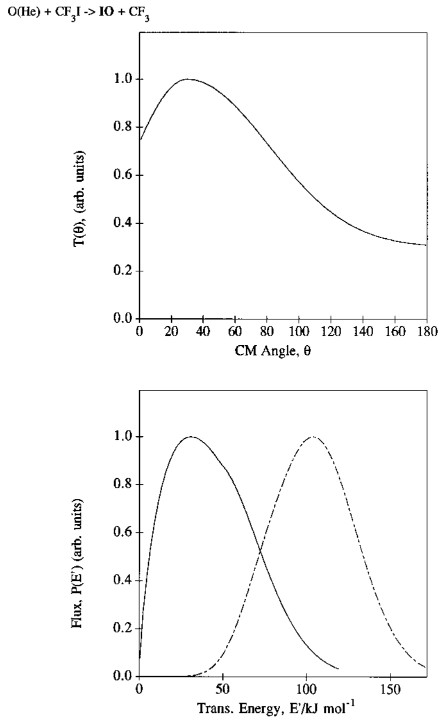

Figure 5. Angular function $T(\theta)$ and translational energy distribution $P(E')$ for IO product from O + CF$_3$I at initial translational $E \sim 108$ kJ mol^{-1}. The dot-dashed energy curve shows the distribution of initial translational energy.

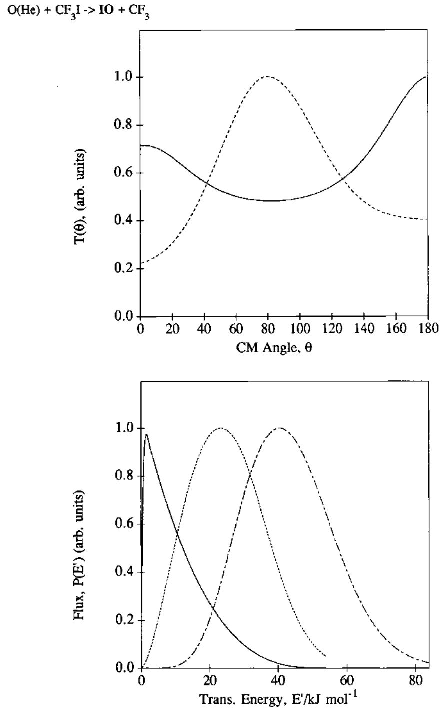

Figure 6. Angular functions $T(\theta)$ and translational energy distributions $P(E')$ for IO products from O + CF$_3$I at initial translational energy $E \sim 42$ kJ mol^{-1}. The dotted product translational energy distribution corresponds to the sideways peaked angular distribution shown by a dotted curve and the solid product translational energy distribution to the forward and backward peaked angular distribution shown by a solid curve.

Discussion

The IO reactive scattering observed in these experiments shows the O + CF$_3$I reaction holding a position intermediate between the O + C$_2$H$_5$I reaction,[1] which has both rebound scattering over the triplet potential energy surface and long-lived complex dynamics over the singlet potential energy surface, and the O + ICl reaction,[10] which shows only collision complex dynamics up to an initial translational energy $E \sim 100$ kJ mol^{-1}. The potential energy profiles for bent OIR configurations in Figure 7 show the intersection of the triplet ^{3}A$''$ and singlet ^{1}A$'$ potential energy surfaces in the entrance valley. The intersection of these potential energy surfaces is shown as a function of interbond angle β in Figure 8. The lowest triplet

TABLE 2: Reaction Energetics/kJ mol^{-1}, Initial Translational Energy E, Peak Product Translational Energy E'_{pk}, Average Product Translational Energy E'_{av}, and Reaction Exoergicity ΔD_o[a]

E	E'_{pk}	E'_{av}	ΔD_o	eq
108	30	45	10 ± 10	1a
42	23	25	− 18 ± 10	1b
	2	11		

[a] Product translational energies are shown for both components of the scattering at $E = 42$ kJ mol^{-1}.

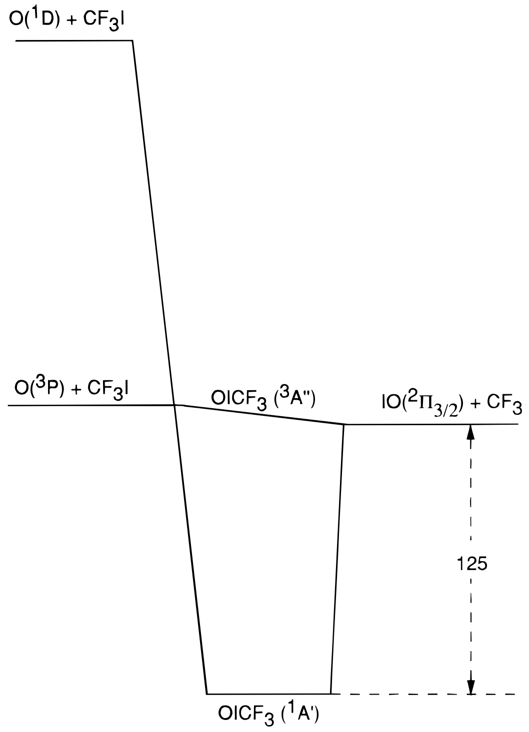

Figure 7. Potential energy profiles for the O + CF$_3$I reaction in bent OICF$_3$ configurations showing the intersection of the lowest singlet and triplet potential energy surfaces. The well depth of the singlet OICF$_3$ complex is estimated to be $E_o = 125 \pm 10$ kJ mol^{-1} with respect to products.

potential energy surface has $^3\Pi$ symmetry in the collinear configuration and splits under Renner Teller interaction[18] on bending to give an upper $^3A'$ potential energy surface which strongly favors the collinear configuration and a $^3A''$ potential energy surface which favors the collinear configuration only weakly and may give rise to a minimum in bent configurations. The singlet $^1A'$ potential energy surface strongly favours bent configurations but may lie above the triplet $^3A''$ potential energy surface in the collinear configuration. The form of these potential energy surfaces depends upon bond length with the singlet $^1A'$ potential energy surface falling well below the triplet potential energy surfaces in strongly bent configurations of the OIR intermediate with contracted bond lengths. This situation is confirmed by the *ab initio* calculations of Marshall[19] for R = CH$_3$ and CF$_3$, where an interbond angle $\beta = 104°$ is estimated for the singlet OICH$_3$ complex.

The sideways scattered component observed at an initial translational energy $E \sim 42$ kJ mol^{-1} is associated with a higher product translational energy than the forward and backward scattered component in Figure 6. This suggests that the sideways scattered component may be associated with direct reaction over the triplet $^3A''$ potential energy surface with the O(^{3}P) atom approaching broadside[20] to the CF$_3$I molecule, while the forward and backward scattered component is associated with a persistent OICF$_3$ complex on the singlet $^1A'$ potential energy surface. A long-lived OICF$_3$ complex dissociating without any intervening potential energy barrier should yield a product translational energy distribution in accord with phase space theory.[21-23] The phase space product translational energy distribution calculated with maximum initial $b_m = 2.5$ Å and final $b'_m = 5.0$ Å impact parameters and seven vibrational modes[24,25] shows good agreement with the experimental distribution for the forward and backward peaked component in Figure 9. However it falls well below the product translational energies for the sideways scattered component and the corresponding phase space calculation carried out at an initial translational energy $E \sim 108$ kJ mol^{-1} also falls well below the experimental distribution in Figure 10. This suggests that the conical scattering into the forward hemisphere observed in Figure 5 at an initial translational energy $E \sim 108$ kJ mol^{-1} arises primarily from direct reaction over a triplet $^3A''$ potential energy surface. Hence the reactive scattering observed in these

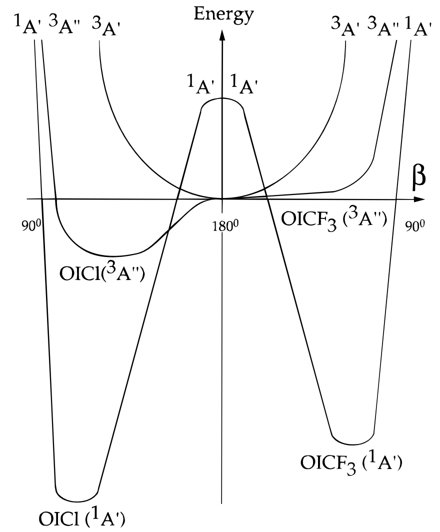

Figure 8. Schematic correlation diagram for triplet states with Renner Teller interaction and the singlet state in bent OICF$_3$ configurations with interbond angle β (right-hand side) compared with OICl (left hand side). Symbols refer to the electronic symmetry about the OIC and OICl bonds.

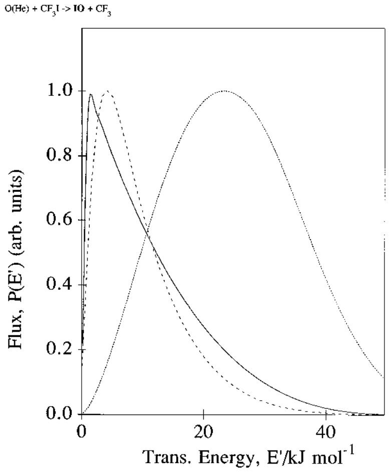

Figure 9. Product translational energy distribution calculated from phase space theory (broken curve) compared with the experimental scattering distributions (solid and dotted curves) for the O + CF$_3$I reaction at initial translational energy $E \sim 42$ kJ mol^{-1}. The uncertainties in the experimental peak product translational energies are ~3 kJ mol^{-1} and ~1 kJ mol^{-1} for the fast and slow components, respectively.

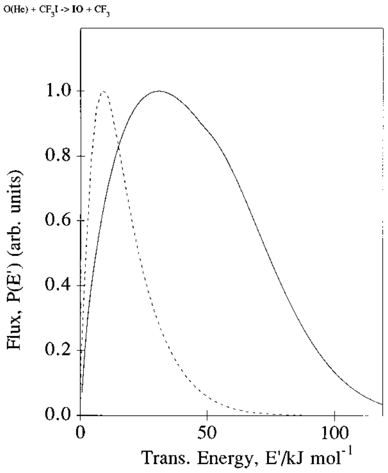

Figure 10. Product translational energy distribution calculated from phase space theory (broken curve) compared with the experimental distribution (solid curve) for O + CF_3I at initial translational energy $E \sim 108$ kJ mol^{-1}.

TABLE 3: Nominal Crossing Radii r_c Calculated from Eq 5 with Ionization Potential I(IO) = 9.6 eV and Electron Affinities A(R) compared with Bond Lengths r_e (RI)

RI	A(R)/eV	r_c/Å	r_e/Å
CH_3I	~0	1.5	2.14
CF_3I	1.78	1.8	2.13
ICl	3.613	2.4	2.32

experiments at high initial translational energy confirms a transition in the dynamics of the O + CF_3I reaction from the long-lived complex mechanism observed by Buss *et al.*[6] at the lowest initial translational energy $E \sim 10$ kJ mol^{-1} through an increasing contribution of a direct reaction mechanism, which was poorly resolved by previous measurements[5,26] at intermediate initial translational energy $E \sim 15-30$ kJ mol^{-1} but which is now clearly resolved in the scattering at higher initial translational energy $E \sim 40-110$ kJ mol^{-1}.

Matrix isolation measurements[7-9] show the existence of a bound OIR intermediate, which may be identified with the minimum on the singlet $^1A'$ potential energy surface. Infrared measurements of the matrix isolated OIR intermediate show that the vibrational frequency of the OI bond depends upon the identity of the R group. This is attributed to the contribution of charge transfer interaction of the form OI^+R^-, which is most pronounced[27] for R = Cl. The IO^+ ion has $^3\Sigma^-$ symmetry, so that the effect of charge transfer interaction is expected to be most pronounced in lowering the triplet $^3A''$ potential energy surface in bent configurations since the charge transfer state also has $^3A''$ symmetry. The low lying $IO^+(^1\Delta)$ electronically excited state may also contribute to charge transfer interaction with the singlet $^1A'$ potential energy surface in strongly bent configurations.

The estimated ionization potential of the IO radical, $I(IO) \sim 9.6$ eV, greatly exceeds the electron affinities[28-30] A(R) of the R radicals listed in Table 3. Hence the $IO^+ + R^-$ ion pair state lies well above the covalent IO + R reaction products at large internuclear distance. The potential energy of the ionic state is lowered by Coulomb attraction to that of the covalent state at the internuclear distance of the nominal crossing radius

$$r_c = e^2/4\pi\epsilon_0[I(IO) - A(R)] \tag{5}$$

The values of r_c given in Table 3 show that the charge transfer interaction makes a significant contribution to the ground state triplet wavefunction only when the $OI^+- - R^-$ internuclear distance has decreased to approximately the equilibrium bond length[18,31] of the IR reactant molecule. Consequently the charge transfer stabilization of the OIR intermediate will decline rapidly in both the entrance and exit valleys of the triplet $^3A''$ potential energy surface. This situation is confirmed by the matrix isolation measurements of the IO vibrational frequency of the OIR intermediate, which indicate an increase of frequency with the electron affinity of the R radical. Hence the charge transfer stabilization of the $^3A''$ potential energy surface in bent OIR configurations will be most pronounced for R = Cl and this may influence the intersection with the singlet $^1A'$ potential energy surface as shown in Figure 8.

The probability of intersystem crossing in the entrance valley of the triplet $^3A''$ potential energy surface with an extended O−IR internuclear distance is characterized by the weak spin−orbit interaction of the O(^{3}P) atom. Consequently the intersystem crossing probability arising from a single traversal of the seam of intersection is expected to be low, independent of the identity of the R radical. However, the strength of spin−orbit interaction at the seam of intersection of the OIR intermediate shown in Figure 8 will be increased by the transfer of spin density to the heavy I atom as the OI bond contracts. Hence the intersystem crossing probability increases for subsequent traversals of the seam of intersection. Consequently, high probabilities of intersystem crossing may accumulate for trajectories which involve multiple crossings of the seam of intersection. This situation is reflected in the predominance of direct scattering over the $^3A''$ potential energy surface for O + CF_3I at higher initial translational energy. The sideways scattering in Figure 6 with high product translational energy indicates that the transition state is strongly bent on the triplet $^3A''$ potential energy surface, which does not support a potential energy minimum as shown in Figure 7. However, the continuation of long-lived complex dynamics[10] up to the highest initial translational energy for O + ICl suggests that in this case the triplet $^3A''$ potential energy surface supports a minimum in strongly bent configurations, resulting in trapped trajectories and a sustained high probability of intersystem crossing to the singlet $^1A'$ potential energy surface.

The *ab initio* calculations of Marshall[19] predict a well depth $E_0 \sim 125$ kJ mol^{-1} with respect to products for the singlet $OICF_3$ complex as shown in Figure 7. Hence the ratio of the lifetime τ to the rotational period τ_{rot} may be estimated for the singlet $OICF_3$ complex from the RRKM formula[32]

$$\frac{\tau}{\tau_{rot}} \cong \frac{L_m}{2\pi I_2^* \nu}\left(\frac{E + \Delta D_0 + E_0}{E + \Delta D_0}\right)^{s-1} \tag{6}$$

This yields $\tau \sim 5\tau_{rot}$ for $E = 42$ kJ mol^{-1} and $\tau \sim 2.5\tau_{rot}$ for $E = 108$ kJ mol^{-1} when using a maximum initial orbital angular momentum $L_m = 140\ \hbar$, a moment of inertia $I_2^* = 6.3 \times 10^{-45}$ kg m^2, a mean vibrational frequency $\nu = 1.1 \times 10^{13}$ s^{-1}, and an effective number of vibrational modes $s = 7$. Consequently the singlet $OICF_3$ complex is expected to be long lived with respect to its rotational period, even at the higher initial translational energy of these experiments. The mild forward and backward peaking of the IO scattering from the singlet $OICF_3$ complex in Figure 6 corresponds to intersystem crossing occurring in collisions at small impact parameters $b < 2.5$ Å with the iodine atom end of the reactant CF_3I molecule. The mild preference for backward scattering in Figure 6 suggests that reaction at small impact parameters may be augmented by trajectories which commence in more nearly collinear configurations on the triplet $^3A'$ potential energy surface.[33]

No reactive scattering of CF_3O products from the insertion pathway

$$O + CF_3I \rightarrow CF_3O + I \qquad (7)$$

was detected in these experiments, in accord with recent kinetics measurements.[34] This indicates that a potential energy barrier inhibits rearrangement of the $OICF_3$ complex on the singlet $^1A'$ potential energy surface to the $IOCF_3$ isomer, which would dissociate preferentially according to the strongly exoergic pathway of eq 7 with $\Delta D_o \sim 210$ kJ mol^{-1} estimated from the CF_3O bond energy quoted by Li and Francisco.[35]

Acknowledgment. Support of this work by EPSRC and the European Commission is gratefully acknowledged. We are grateful to Professor P. Marshall for communicating the results of his *ab initio* calculations prior to publication.

References and Notes

(1) Wang, J. J.; Smith, D. J.; Grice, R. *J. Phys. Chem.* **1996**, *100*, 6620.

(2) Wang, J. J.; Smith, D. J.; Grice, R. *J. Phys. Chem.* **1996**, *100*, 13 603.

(3) Klaassen, J. J.; Lindner, J.; Leone, S. R. *J. Chem. Phys.* **1996**, *104*, 7403.

(4) Addison, M. C.; Donnovan, R. J.; Garraway, J. *Discuss. Faraday Soc.* **1979**, *67*, 286.

(5) Gorry, P. A.; Nowikow, C. V.; Grice, R. *Molec. Phys.* **1979**, *38*, 1485.

(6) Buss, R. J.; Sibener, S. J.; Lee, Y. T. *J. Phys. Chem.* **1983**, *87*, 4840.

(7) Andrews, L.; Hawkins, M.; Withnall, R. *Inorg. Chem.* **1985**, *24*, 4234.

(8) Hawkins, M.; Andrews, L. *Inorg. Chem.* **1985**, *24*, 3285.

(9) Clark, R. J. H.; Dann, J. R. *J. Phys. Chem.* **1996**, *100*, 532.

(10) Powell, L. J.; Wells, D. D.; Wang, J. J.; Smith, D. J.; Grice, R. *Molec. Phys.* **1996**, *87*, 865.

(11) Pollard, J. E. *Rev. Sci. Instrum.* **1992**, *63*, 1771.

(12) Gorry, P. A.; Grice, R. *J. Phys. E* **1979**, *12*, 857.

(13) Nowikow, C. V.; Grice, R. *J. Phys. E* **1979**, *12*, 515.

(14) Balucani, N.; Beneventi, L.; Casavecchia, P.; Volpi, G. G. *Chem. Phys. Lett.* **1991**, *180*, 34.

(15) Entemann, E. A.; Herschbach, D. R. *Discuss. Faraday Soc.* **1967**, *44*, 289.

(16) Radlein, D. St. A. G.; Whitehead, J. C.; Grice, R. *Nature London* **1975**, *253*, 37.

(17) Okafo, E. N.; Whittle, E. *Intl. J. Chem. Kinetics* **1975**, 7, 273.

(18) Herzberg, G. *Electronic Spectra of Polyatomic Molecules*; Van Nostrand Reinhold: New York, 1966.

(19) Marshall, P., private communication.

(20) Rochford, J. J.; Powell, L. J.; Grice, R. *J. Phys. Chem.* **1995**, *99*, 15 369.

(21) Pechukas, P.; Light, J. C.; Rankin, C. *J. Chem. Phys.*, **1966**, *44*, 794.

(22) Lin, J.; Light, J. C. *J. Chem. Phys.* **1966**, *45*, 2545.

(23) Light, J. C. *Discuss. Faraday Soc.* **1967**, *44*, 14.

(24) Yamada, C.; Hirota, E. *J. Chem. Phys.* **1983**, *78*, 1703.

(25) Durie, R. A.; Legay, F.; Ramsay, D. A. *Can. J. Phys.* **1960**, *38*, 444.

(26) Steele, T. A. Ph.D. Thesis, University of Manchester, 1985.

(27) Hawkins, M.; Andrews, L.; Downs, A. J.; Dury, D. J. *J. Am. Chem. Soc.* **1984**, *106*, 3076.

(28) Graul, S. T.; Squires, R. R. *J. Am. Chem. Soc.* **1990**, *112*, 2506.

(29) Miller, D. M.; Allen, W. D.; Schaefer, H. F. *Molec. Phys.* **1996**, *88*, 727.

(30) Berry, R. S.; Reimann, C. W. *J. Chem Phys.* **1963**, *38*, 1540.

(31) Huber, K. P.; Herzberg, G. *Constants for Diatomic Molecules*; Van Nostrand Reinhold; New York, 1979.

(32) White, R. W. P.; Smith, D. J.; Grice, R. *J. Phys. Chem.* **1993**, *97*, 2123.

(33) White, R. P. W.; Smith, D. J.; Grice, R. *Chem. Phys. Lett.* **1992**, *193*, 269.

(34) Gilles, M. K.; Turnipseed, A. A.; Talukdar, R. K.; Rudich, Y.; Villalta, P. W.; Huey, L. G.; Burkholder, J. B.; Ravishankara, A. R. *J. Phys. Chem.* **1996**, *100*, 14 005.

(35) Li. Z.; Francisco, J. *J. Am. Chem. Soc.* **1989**, *111*, 5660.